

An Assessment of the Seasonal Salinity Budget for the Upper Bay of Bengal

EARLE A. WILSON AND STEPHEN C. RISER

School of Oceanography, University of Washington, Seattle, Washington

(Manuscript received 7 August 2015, in final form 27 January 2016)

ABSTRACT


During each summer monsoon, the Bay of Bengal is inundated by a large amount of rain and river discharge. The effects of this freshening are gradually reversed over the course of the year, with near-surface salinities typically returning to their presummer monsoon levels before the start of the next rainy season. While the forcing responsible for the summertime freshening is clear, the processes that act to restore the bay's salinity are not well understood. To examine these processes, the authors construct a basin-integrated, near-surface, seasonal salinity budget using data-assimilated output from the Hybrid Coordinate Ocean Model (HYCOM). From this salinity budget, it is deduced that vertical salt fluxes are primarily responsible for counterbalancing the near-surface freshening caused by the summertime freshwater fluxes. These vertical salt fluxes are largest during the months that immediately follow the summer monsoon, when the near-surface halocline is strongest. These results must be tempered with the knowledge that HYCOM misrepresents some key features of the bay's salinity field. In particular, the model tends to overestimate salinity along the East Indian Coastal Current during its equatorward phase. Notwithstanding these biases, these results still suggest that vertical processes have a prominent role in the bay's near-surface salinity budget.

1. Introduction

The variability of salinity in the Bay of Bengal (BoB) has significant influence over a wide range of physical processes in the region. This influence is mainly derived from the role salinity plays in setting the bay's near-surface stratification. In the upper 50 m of the bay, salinity rapidly increases with depth and often forms a strong halocline near the surface (e.g., [Shetye et al. 1996](#); [Thadathil et al. 2007](#)). The presence of this near-surface halocline sets a relatively shallow mixed layer and supports the existence of subsurface barrier layers ([Vinayachandran et al. 2002](#); [Thadathil et al. 2007](#)). These barrier layers separate the surface mixed layer from the main thermocline and permit temperature inversions to exist below the mixed layer ([Girishkumar et al. 2013](#)). Thus, through its strong control over the

vertical distribution of heat in the bay's near-surface layers, salinity variability in the BoB can indirectly affect processes such as the active-break cycles of the summer monsoon ([Sengupta et al. 2001](#); [Vecchi and Harrison 2002](#)) and the development of regional tropical cyclones ([Sengupta et al. 2008](#); [Neetu et al. 2012](#)).

Given the importance of salinity in the BoB, many studies have sought to better understand the nature of its seasonal variability. From these efforts, we learn that the northern BoB features the most extreme salinity variability in the northern Indian Ocean ([Rao and Sivakumar 2003](#); [Sharma et al. 2010](#)). This is mainly due to the immense seasonal discharge from rivers such as the Ganges, Brahmaputra, and the Irrawaddy. Studies have also shown that surface currents play an important role in the redistribution of freshwater within the bay ([Rao and Sivakumar 2003](#); [Nyadjro et al. 2010](#)). In particular, the East Indian Coast Current (EICC) has been identified as a major mechanism for freshwater export from the BoB to the greater Indian Ocean (e.g., [Shetye et al. 1996](#); [Akhil et al. 2014](#); [Chaitanya et al. 2014](#)). Additionally, more recent studies have elevated the importance of vertical mixing in the near-surface salinity budget (e.g., [Vinayachandran et al. 2013](#); [Benshila et al. 2014](#); [Akhil et al. 2014](#)). These studies advance the notion that vertical

 Denotes Open Access content.

Corresponding author address: Earle Wilson, School of Oceanography, University of Washington, Box 357940, Seattle, WA 98195.

E-mail: earlew@uw.edu

DOI: 10.1175/JPO-D-15-0147.1

salt fluxes play a critical role in restoring the salinity of the near-surface after the summer monsoon freshening.

Despite this progress, many important questions concerning the seasonality of the bay's near-surface salinity remain unsatisfactorily answered. While we know that the freshwater fluxes associated with the summer monsoon will act to decrease near-surface salinity, we do not fully understand the mechanisms that act to compensate for those changes. The pathways of freshwater water export from the BoB are also unclear. Though the freshwater flux by the EICC has received much attention, the variability and magnitude of freshwater export elsewhere, particularly in the Andaman Sea, are largely unconstrained. Additionally, the importance of vertical mixing in maintaining the near-surface salinity balance is unsettled. Some studies have suggested that salinity transport in the bay occurs mostly in the horizontal plane and that the effect of vertical mixing is negligible (e.g., Rao and Sivakumar 2003), while other studies have proposed that vertical mixing is a leading-order process controlling near-surface salinity (e.g., Vinayachandran et al. 2013; Benshila et al. 2014; Akhil et al. 2014).

To address these lingering questions, we consider a basin-integrated, seasonal, near-surface salinity budget that accounts for both horizontal and vertical salinity fluxes. Although a few studies have analyzed salinity variability for different subregions of the bay (e.g., Akhil et al. 2014; Pant et al. 2015; D'Addezio et al. 2015), there has yet to be a complete, basin-integrated salinity budget analysis for the entire BoB region. By including the entire basin in our analysis, we are able to directly account for freshwater input from both rainfall and continental discharge. This approach allows us to evaluate how the cumulative effect of ocean processes balances the net effect of freshwater fluxes on near-surface salinity.

A major hindrance to establishing such a budget is the paucity of in situ data in the BoB. In particular, very little data exist for the coastal regions of the bay and the Andaman Sea. To work around these limitations, we turn to data-assimilated model output from the Hybrid Coordinate Ocean Model (HYCOM). We choose HYCOM because it is a widely used, state-of-the-art, high-resolution ocean model that has been thoroughly validated in other parts of the ocean (Chassignet et al. 2007). The reliability of HYCOM is bolstered by its data assimilation scheme that incorporates almost all publicly available in situ and remotely sensed ocean data. In the BoB, assimilated data mainly come from profiling floats, moorings, and satellite estimates of sea surface temperature (SST) and sea surface height (SSH). Since HYCOM assimilates data, we consider its ocean state estimates to be more akin to other observationally based gridded data products, such as optimally interpolated

gridded Argo data, more so than purely dynamical model output, such as the simulations described in Akhil et al. (2014). The main conceptual difference between this HYCOM product and other observationally based gridded datasets is the manner in which data are interpolated. In our case, HYCOM essentially acts as a “dynamic interpolator” of ocean data as it combines a vast array of observational data to produce ocean state estimates that are consistent with the dynamical constraints of the ocean.

Our paper is outlined as follows: In section 2, we discuss the data and model output used in this study. In section 3, we provide a glimpse of the seasonal variability of the northern Indian Ocean, as simulated by HYCOM, with a special focus on the BoB. In section 4, we assess the validity of HYCOM's salinity output in the BoB by comparing the model's estimates with Argo data. In section 5, we derive a salinity budget for the upper BoB region and discuss how HYCOM's data assimilation and sea surface salinity (SSS) relaxation schemes affect our analysis. In sections 6 and 7, we present and discuss the results of our budget analysis. In sections 8 and 9, we provide our summary and conclusions.

2. Model output and data

a. HYCOM + NCODA global analysis

HYCOM is a primitive equation, ocean general circulation model that solves five prognostic equations—two horizontal momentum equations, one mass continuity equation, and two conservation equations for a pair of thermodynamic variables (Bleck 2002). The model features a hybrid vertical coordinate system that varies from being isopycnal in the open, stratified ocean; Cartesian in the weakly stratified, near-surface ocean; and terrain following in the proximity of major topographical features. In the upper ocean, vertical coordinates can transform between isopycnal and Cartesian coordinates in response to changes in water column stratification. The main advantage of this hybrid vertical coordinate system is that it permits the use of sophisticated, nonslab mixing schemes in the upper ocean without compromising computational efficiency in the ocean interior. For the model runs discussed here, vertical mixing throughout the water column was parameterized by the K-profile parameterization (KPP) scheme (Large et al. 1994). A detailed description of HYCOM's governing equations, mixing schemes, and numerical algorithms is provided in Bleck (2002).

HYCOM is the centerpiece of the HYCOM Consortium for Data Assimilative Ocean Modeling (Cummings

2005; Metzger et al. 2014). In this system, HYCOM is integrated with an atmospheric general circulation model and an ocean data assimilation scheme to produce near-real-time hindcasts, “nowcasts,” and forecasts of the ocean’s physical state. For the runs used in this study, the model was forced at the surface by the Navy Operational Global Atmospheric Prediction System (NOGAPS). NOGAPS was an atmospheric general circulation model used for short-term weather prediction (Rosmond et al. 2002); it has since been superseded by the Navy Global Environmental Model (NAVGEM) atmospheric model. NOGAPS provided 3-hourly surface forcings of wind stress, wind speed, heat flux, and precipitation. Evaporation and surface heat fluxes are determined using bulk formulae. River discharge was introduced as artificially intense rainfall near the mouth of rivers. The simulated river outflow was based on the river discharge climatology described in Barron and Smedstad (2002). It should be noted that while HYCOM and NOGAPS actively influenced each other, they were not fully coupled, since the NOGAPS output was held fixed during a HYCOM forecast and vice versa.

Data were assimilated using the Navy Coupled Ocean Data Assimilation (NCODA) scheme (Cummings 2005; Metzger et al. 2014). NCODA assimilates a vast array of near-real-time ocean data including in situ temperature and salinity profiles from XBTs, Argo floats, and moored buoys as well as satellite-derived SST and SSH. Within the BoB, in situ data mainly came from Argo profiles scattered throughout the bay and a handful of Research Moored Array for African–Asian–Australian Monsoon Analysis and Prediction (RAMA) moorings in the southeastern region of the bay (McPhaden et al. 2009). We note that while satellite-based SSS has been assimilated in more recent experiments, they were not included in the model runs used in this study. NCODA assimilates data using a multivariate optimal interpolation procedure that is applied both forward and backward in time to ensure smooth adjustments to the model’s state variables. Adjustments are constrained by geostrophic balance such that any adjustment to the density field is coupled with a proportional adjustment in the velocity field and vice versa. In addition to assimilating data, the model also relaxed its SSS values to observed climatology from the Polar Science Center Hydrographic Climatology (PHC) (Steele et al. 2001). In the BoB, PHC is equivalent to the 1998 Levitus climatology.

In this study, we analyze archived HYCOM output from the global, data-assimilated HYCOM $1/12^\circ$ (GLBa0.08) experiments, listed as 90.6, 90.8, and 90.9 on the official HYCOM data server (<http://hycom.org/dataserver/glb-analysis>, accessed August 2014). These experiments span September 2008 to July 2013 and

provide daily, global output of salinity, temperature, and horizontal velocities. These variables were made available on 32 constant z -level surfaces with $\sim 0.08^\circ$ horizontal resolution.

b. Auxiliary data

In addition to the previously described HYCOM experiments, we supplement our analysis with observational data. To test the performance of HYCOM in the region, we compare its output with in situ Argo profile data. These data were obtained from the 2013 edition of the World Ocean Database (WOD2013), and only profiles flagged as “acceptable” were retained for our analysis (Boyer et al. 2013). To determine surface freshwater fluxes, we use observationally derived estimates of evaporation, precipitation, and river discharge. Ocean evaporation data were sourced from the daily, $1^\circ \times 1^\circ$ resolution objectively analyzed air–sea fluxes (OAFlux) dataset (Yu et al. 2008). Precipitation data were obtained from the daily, $0.25^\circ \times 0.25^\circ$ resolution Tropical Rainfall Measuring Mission (TRMM) 3B42 V7 dataset (TRMM 2013). Continental runoff data came from the global river flow and continental discharge dataset (Dai and Trenberth 2002). These runoff estimates were derived using river gauge records and a continental drainage model and were supplied as $1^\circ \times 1^\circ$ gridbox estimates along the continental coastlines. To obtain total discharge into the BoB region, we integrated the continental discharge estimates north of 10°N between 78° and 98°E . Of the auxiliary data mentioned here, only Argo data were assimilated by HYCOM.

3. Northern Indian Ocean variability as simulated by HYCOM

Maps of monthly near-surface salinity and ocean currents demonstrate that HYCOM is able to reproduce the major large-scale features of the northern Indian Ocean (Fig. 1). The model captures the well-known near-surface salinity contrast between the Arabian Sea and the BoB. For our study period, mean SSS in the Arabian Sea and BoB were about 35 and 32 psu, respectively. From HYCOM, we observe that both ocean basins exhibit varying degrees of seasonal SSS variability. In the BoB region, the simulated SSS varies between 34 psu to values much lower than 31 psu, with minimum and maximum values occurring during fall and spring months, respectively. In the Arabian Sea, the seasonal SSS variability is more muted, with typical salinities ranging from about 35.5 to 36.5 psu.

HYCOM produces the expected seasonal surface circulation for the BoB. This is best exemplified by the model’s representation of the biannual reversal of the

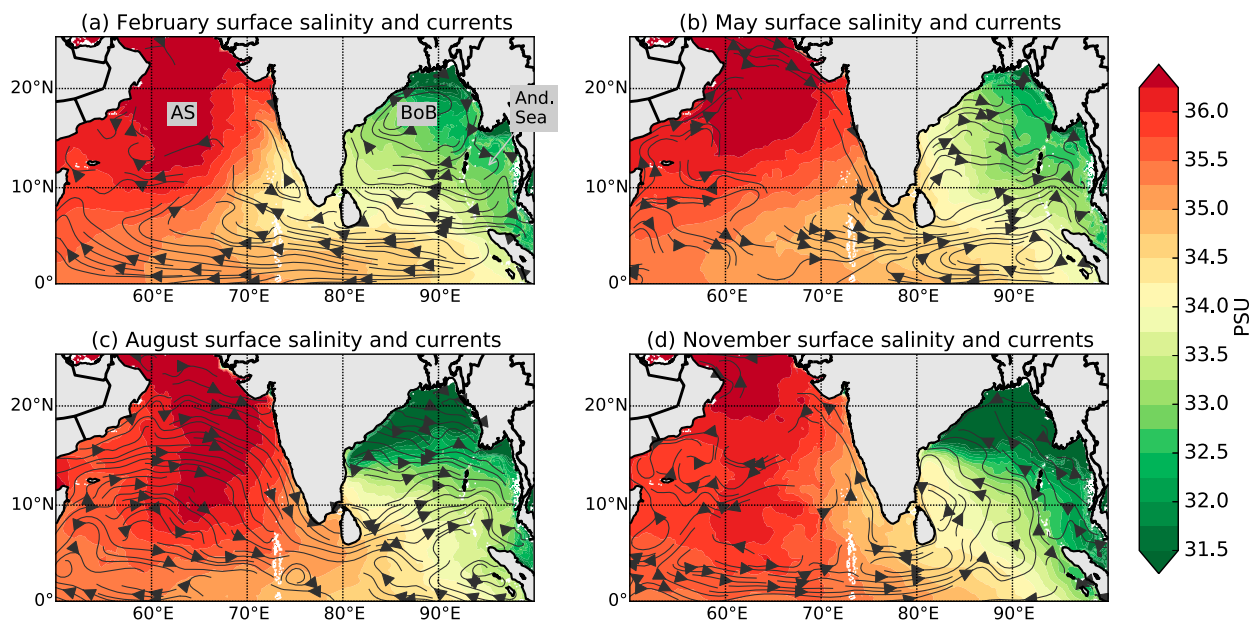


FIG. 1. Plots showing monthly mean surface salinities (colored shading) and currents (streamlines) estimated from HYCOM output for (a) February, (b) May, (c) August, and (d) November. Streamlines are only shown where the local current speed exceeds 0.1 m s^{-1} . (a) This map shows the locations of the Arabian Sea (AS), BoB, and the Andaman Sea (And. Sea).

EICC (Fig. 2). Between roughly September and February at 10°N , the EICC flows equatorward with maximum surface velocities of about -0.75 m s^{-1} . Some of this outflow is recirculated into the bay by a prominent cyclonic eddy situated just northeast of Sri Lanka (Fig. 1d). These features exist within a large-scale, cyclonic, surface circulation pattern that spans most of the bay during the winter monsoon. Between March and July, the EICC flows in the opposite direction, with maximum surface velocities of about 0.5 m s^{-1} and forms the northward branch of the cyclonic surface circulation that extends over most of bay. HYCOM's representation of the EICC is in good agreement with the observationally based surface velocity estimates reported by Shetye et al. (1996) and Durand et al. (2009). However, we note that HYCOM produces slightly weaker surface velocities for the EICC during fall months, compared to observations. Satellite-based measurements of the EICC between years 1992 to 2002 show that maximum surface flow near 10°N regularly exceeded -1 m s^{-1} during fall months (Fig. 4e of Durand et al. 2009). It is unclear whether this reflects a true bias in HYCOM or actual interannual variability.

According to HYCOM's ocean state estimates, the summertime freshening of the BoB extends much deeper than the conventionally defined mixed layer (Fig. 3). Here, the mixed layer depth (MLD) is defined as the depth at which potential density is 0.125 kg m^{-3} greater than at the surface. By this definition, the MLD remains relatively shallow throughout the year, varying between 15 and 35 m with an average depth of around

20 m. However, seasonal variations of salinity are evident down to depths of 80–100 m (Fig. 3).

4. Argo–HYCOM comparisons

Even though HYCOM assimilates a broad range of ocean data, the model is still susceptible to errors and

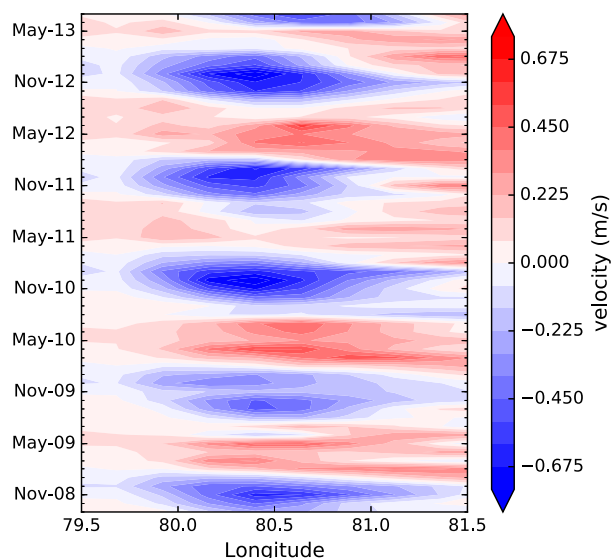


FIG. 2. A Hovmöller plot of northward surface velocities, from HYCOM output, at 10°N between 79.5° and 81.5°E . The velocity estimates at this location represent the seasonally reversing EICC. Contour interval is 0.075 m s^{-1} .

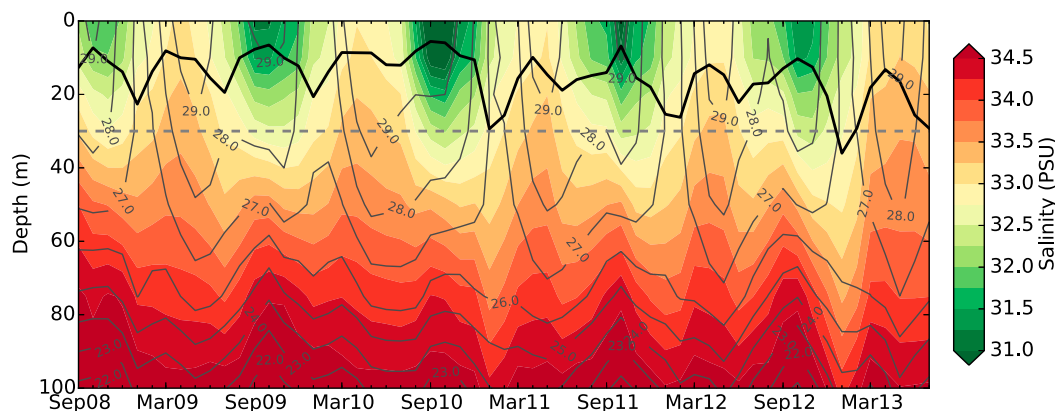


FIG. 3. Monthly mean salinity (shading) and temperature (contour lines) for the upper 100 m of the BoB region (inclusive of the Andaman Sea). These monthly mean sections were estimated from HYCOM output. The solid black line is the mixed layer depth, computed as the depth at which potential density is 0.125 kg m^{-3} greater than at the surface. The flat broken line is the 30-m depth level, which is used as the base of our control volume in our budget analysis.

biases. For this reason, we compare HYCOM's salinity estimates with in situ salinity measurements from Argo profiling floats. Since HYCOM assimilates Argo data, these profiling data are not an independent reference, but, as we will show, there are significant differences between the final assimilated output and the in situ data.

Between September 2008 and July 2013, Argo floats produced over 6000 profiles of salinity in the BoB region (Fig. 4). Almost all profiles were collected west of the Andaman Islands, and the number of profiles collected in the bay generally increased over our study period. In the year 2009, the average monthly profile count was about 250 profiles per month; by 2012, over 1000 profiles were collected each month (Fig. 4b).

To assess HYCOM's performance, we compare the model's gridbox salinity estimates with any available collocating and cooccurring Argo profile measurements. We eschew any form of objective mapping as this process tends to smooth important small-scale features, such as coastal currents and density fronts. The obvious drawback to this approach is that in situ measurements are subject to high-frequency, subgrid-scale processes that HYCOM cannot directly resolve. However, we are primarily concerned with large-scale, systematic biases in HYCOM's output that may affect our analysis. These biases, if they exist, should form clear patterns in the otherwise noisy error fields.

Monthly maps of the differences between HYCOM's gridbox salinity estimates and collocated Argo salinity profiles reveal coherent patterns of disagreement (Fig. 5). This coherence suggests a systematic source of error. Between February and May, HYCOM

simulated higher, near-surface salinity estimates than what was measured by Argo. These differences are greatest in the northern BoB, where the maximum disparities are on the order of 1 psu. This average discrepancy is well above the accuracy of Argo's salinity measurements, which is generally taken to be 0.01 psu (Riser et al. 2008). In August, which is representative of all summer months, HYCOM's near-surface salinity shows no clear bias. However, for November, a strip of positive salinity biases (in excess of 1 psu) is evident along the southwestern coastline of the bay. These biases are also apparent at the 50-m depth level. This indicates that HYCOM tends to overestimate the salinity of the EICC during the winter monsoon. This could mean that the model entrained too much high salinity from water from offshore regions. Another likely source of error is the SSS relaxation process since the reference SSS climatology used in this scheme is too coarse to capture this narrow low-salinity plume.

Away from the western boundary, at the 50-m depth level, HYCOM's salinities are generally lower than those from Argo. These findings support previous reports of negative, subsurface salinity biases in HYCOM output for the BoB (D'Addezio et al. 2015). This subsurface bias is largest in November and has maximum magnitude in the northern regions of the bay. For February through May, the negative salinity biases at 50-m depth are associated with positive salinity biases near the surface. This suggests that the model is overestimating the strength of vertical mixing in the upper bay for those months and possibly for other times of the year. In a later section, we evaluate how all these biases affect our budget analysis.

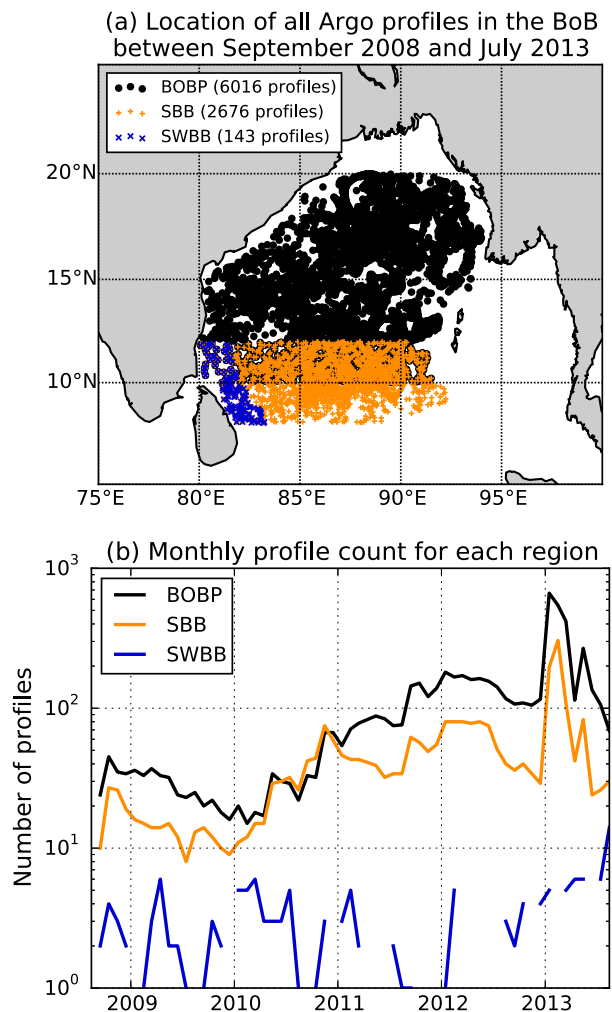


FIG. 4. (a) Map showing positions of all Argo profiles in the BoB between September 2008 and July 2013. The profiles are grouped into three subregions: BOBP, black circles; SBB, orange crosses; and SWBB, blue crosses. The BOBP subregion accounts for profiles north of 10°N. The SBB subregion accounts for all profiles found between 8° and 12°N. The SWBB subregion accounts for the SBB profiles within 2° of the Indian/Sri Lankan coastline. The number of profiles available for each region is provided in the legend. Gray circles show profiles from the Andaman Sea. (b) Time series of monthly profile count for each region.

5. Upper BoB salinity budget

a. Budget derivation

For our salinity budget, we define a control volume that spans the oceanic region north of 10°N, enclosed by the eastern coast of India and the western coast of the Malay Peninsula. This definition of the BoB includes the Andaman Sea, which is not formally a part of the BoB. The advantage of this loose definition is that it allows us to eliminate zonal salt fluxes from our budget. For clarification, we will refer to the “BoB proper” as

the conventionally defined BoB that excludes the Andaman Sea. The control volume is bounded by the 30-m depth level, which is slightly deeper than the mean MLD of the bay (Fig. 3). We choose a fixed-depth level for its simplicity but acknowledge that the choice of this depth level is somewhat arbitrary. However, the major conclusions presented in this paper are qualitatively true for control volume depths ranging between 20 and 40 m.

A salt budget for this control volume may be defined by

$$\frac{\partial}{\partial t} \iiint_{\mathcal{V}} \rho S d\mathcal{V} \simeq \iint_{x,z} \rho S v dz dy \Big|_{y=10^\circ\text{N}} + \iint_{x,y} \rho S w dy dx \Big|_{z=30\text{m}}, \quad (1)$$

where S is salinity, ρ is density, v is northward velocity, w is vertical velocity, and \mathcal{V} is the volume of our control region. The volume \mathcal{V} is assumed to be fixed. At this stage, we make no distinction between resolved and unresolved fluxes in the model. The left side of Eq. (1) represents the rate of change of salt content (salt tendency) within the control volume, while the terms on the right represent the flux of salt into the control volume. The first flux term is the total horizontal salt flux into the upper bay across 10°N, and the second flux term is the total vertical salt flux across the 30-m depth level. Excluded from our budget are salt fluxes due to molecular diffusion. On seasonal time scales, these fluxes are orders of magnitude smaller than the salt fluxes due to advection.

While conceptually simple, Eq. (1) poses some practical challenges. First, the HYCOM database does not provide estimates of vertical velocity, and even if they were available, vertical mixing occurs at a scale that the model cannot directly resolve. Second, Eq. (1) in its current form does not account for freshwater fluxes, since the addition or removal of freshwater from the ocean can only affect the total volume and not the salt content. If we allow \mathcal{V} to vary in response to the addition or removal of freshwater, we could rewrite Eq. (1) to include a term that accounts for the salinity changes due to the expansion or contraction of our control volume. However, in HYCOM, freshwater fluxes are parameterized as “virtual salt fluxes,” whereby the effect on salinity is captured but the associated volume changes are ignored (Huang 1993; Schiller and Kourafalou 2010). Because of these limitations, we reformulate Eq. (1) to better suit our needs.

We simplify Eq. (1) by exploiting the fact that salinity in the upper BoB typically varies between 29 and 35 psu (~17%–20% variability relative to the mean),

HYCOM minus Argo salinity

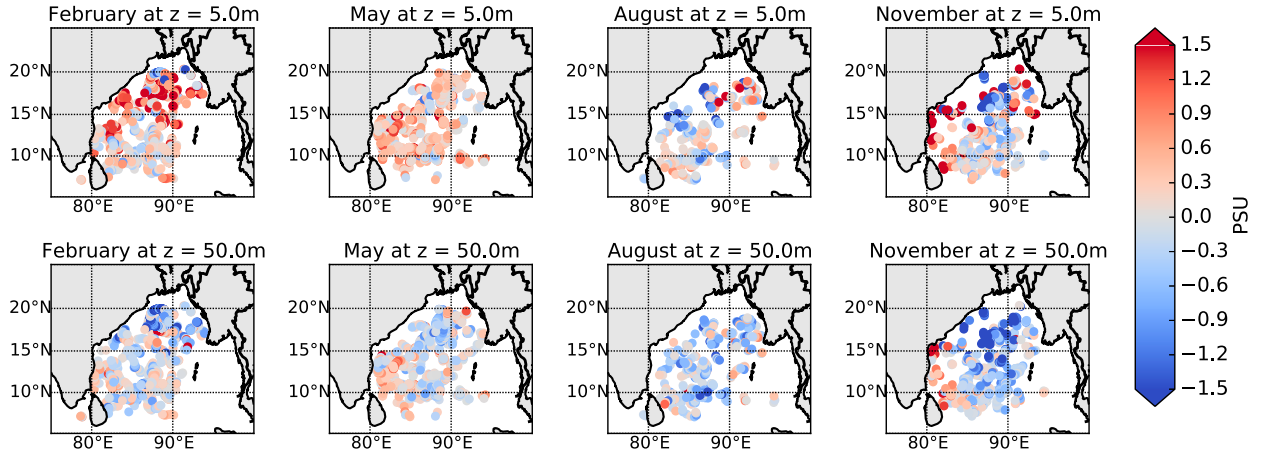


FIG. 5. Maps showing the differences between HYCOM gridbox salinity estimates and collocated Argo profile measurements. (top) HYCOM–Argo differences at 5-m depth level for February, May, August, and November. (bottom) As in (top), but for the 50-m depth level.

while density only varies between 1019 and 1025 kg m^{-3} ($<1\%$ variability relative to the mean). This allows us to treat density as constant and eliminate ρ from our equation. Further, if we divide both sides of our equation by \mathcal{V} , we can interpret each term as volume/area averages instead of volume/area sums:

$$\frac{\partial}{\partial t} \left(\frac{1}{\mathcal{V}} \iiint_{\mathcal{V}} S d\mathcal{V} \right) \simeq \int_{x,z} S v dz dy \Big|_{y=10^\circ\text{N}} + \int_{x,y} S w dy dx \Big|_{z=30\text{m}}, \quad (2)$$

$$\frac{\partial \bar{S}}{\partial t} \simeq \frac{1}{\mathcal{V}} \int_{x,z} S v dz dy \Big|_{y=10^\circ\text{N}} + \frac{1}{\mathcal{V}} \int_{x,y} S w dy dx \Big|_{z=30\text{m}}, \quad \text{and} \quad (3)$$

$$\frac{\partial \bar{S}}{\partial t} \simeq \frac{1}{L_y} \bar{S} v^{x,z} \Big|_{y=10^\circ\text{N}} + \frac{1}{L_z} \bar{S} w^{x,y} \Big|_{z=30\text{m}}. \quad (4)$$

In the last equation, \bar{S} is the volume-averaged salinity of the upper BoB control volume, while $\bar{S} v^{x,z}$ and $\bar{S} w^{x,y}$ are the salinity fluxes averaged across 10°N and $z = 30 \text{ m}$, respectively. The terms L_y and L_z are the length scales of the bay in the y and z directions. The last series of steps had the effect of converting our salt budget to a salinity budget. We can further decompose the right side of Eq. (4) by splitting v and w into a spatial mean component and spatially varying component: $v = \bar{v} + v_0$ and $w = \bar{w} + w_0$. A nonzero, basin-mean vertical velocity can occur if there is basinwide Ekman upwelling or downwelling. By volume conservation, the mean horizontal transport into the control volume must be equal to the total mean vertical transport out of the control volume.

A cursory examination of the v_0 computed from HYCOM's output reveals that there is a relatively large horizontal mean flow into the upper bay on seasonal time scales (Fig. 6). This mean northward flow has an annual average of about 0.04 m s^{-1} . This would translate into $\sim 5 \text{ m yr}^{-1}$ rise in sea level if there was no mean flow through the base of the control volume. Since this rate of sea level rise is unrealistic, the mean northward flow into the upper Bay must be largely balanced by a mean downward flow. Following this logic, v_0 and w_0 are related by

$$w_0|_{z=30\text{m}} = -(L_z/L_y) v_0|_{y=10^\circ\text{N}}. \quad (5)$$

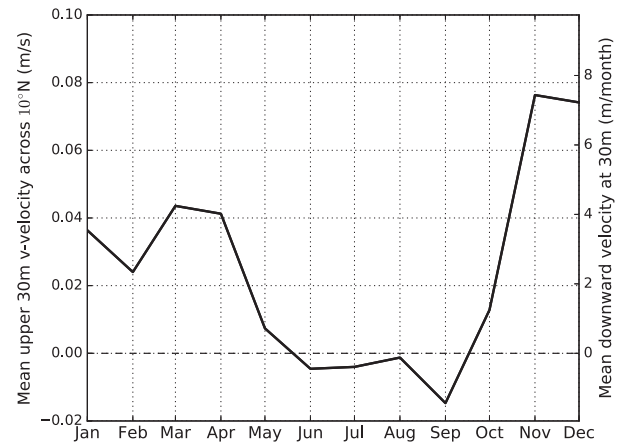


FIG. 6. Left y axis indicates the monthly mean, upper 30m, northward velocity (m s^{-1}) averaged across 10°N . Right y axis indicates the basin-averaged downward vertical velocity (m month^{-1}) at 30m using Eq. (5); here, positive values imply downward motion. Estimates are derived from HYCOM velocity output.

Here, we note that the model is likely underestimating the rate of downwelling since the virtual salt flux parameterization does not account for the pumping caused by the addition of freshwater to the water column (Roullet and Madec 2000). We expect this freshwater-induced pumping to be largest during the summer months, when the basin-averaged freshwater flux is roughly the same order of magnitude as the basin-averaged vertical velocities estimated by Eq. (5) (Fig. 6). However, for the rest of the year, we expect that wind-driven pumping will dominate vertical motion at the 30-m depth level.

Equation (5) allows us to rewrite Eq. (4) as

$$\frac{\partial \bar{S}}{\partial t} \simeq \left. \frac{\overline{Sv}^{x,z}}{L_y} \right|_{y=10N} + \left. \frac{\overline{Sw}^{x,y}}{L_z} \right|_{z=30m} + \frac{v_0|_{y=10N}}{L_y} (\bar{S}^{x,z}|_{y=10N} - \bar{S}^{x,y}|_{z=30m}). \quad (6)$$

Finally, we add a term to account for the salinity changes of our control volume due to surface freshwater fluxes. With the virtual salt flux parameterization, the salinity change or tendency of a single grid box of height h due to some surface freshwater flux F_w is given by

$$\frac{\partial S}{\partial t} = -\frac{F_w S}{h}. \quad (7)$$

Incorporating the above equation into Eq. (6), we get

$$\frac{\partial \bar{S}}{\partial t} \simeq \left. \frac{\overline{Sv}^{x,z}}{L_y} \right|_{y=10N} + \left. \frac{\overline{Sw}^{x,y}}{L_z} \right|_{z=30m} + \frac{v_0|_{y=10N}}{L_y} (\bar{S}^{x,z}|_{y=10N} - \bar{S}^{x,y}|_{z=30m}) - \frac{\bar{F}_w \bar{S}^{x,y}}{L_z}, \quad (8)$$

where $F_w = P + R - E$ (P is precipitation, R is runoff, and E is evaporation). In more simple terms, we can express Eq. (8) for a single month as

$$\Delta \bar{S} \simeq \Delta S_{\text{hmix}} + \Delta S_{\text{vmix}} + \Delta S_{\text{mf}} + \Delta S_{\text{fwf}}, \quad (9)$$

where $\Delta \bar{S}$ is the salinity tendency of our upper BoB control volume. This will be the volume-mean rate of change of salinity for a given month as simulated by HYCOM. The term ΔS_{hmix} represents the salinity tendency of the control volume due to horizontal mixing or advection across 10°N. This term captures the effect of near-surface water mass exchange between the BoB and the greater Indian Ocean. The term ΔS_{vmix} represents the salinity tendency due to vertical salt fluxes across the $z = 30$ -m depth level; ΔS_{mf} accounts for the salinity tendency due to any mean flow in the vertical plane. If there is mean downwelling (upwelling) across the upper bay, by

volume conservation there must be mean flow into (out of) the bay. Finally, ΔS_{fwf} represents the salinity change of the upper bay due to surface freshwater fluxes.

For our analysis, we will compute all terms in Eq. (9) except ΔS_{vmix} . The term ΔS_{vmix} is composed of both unresolved vertical mixing and resolved vertical advection. The former may be represented as $-\overline{\kappa_z}(\partial \bar{S} / \partial z)^{x,y}$, where κ_z is a vertical eddy diffusivity coefficient. In the model, this coefficient is determined using the KPP vertical mixing scheme and is expected to vary in time and space. Unfortunately, we do not have access to the values of κ_z , so we are unable to compute this term directly. With no reliable means of estimating ΔS_{vmix} , we resort to inferring its importance from the residual of our salinity budget.

b. Effects of data assimilation and SSS relaxation

For many models, there is a trade-off between dynamical consistency and truthfulness to observations. A model that is freely evolving would allow for precise diagnostics, since all variability in the model's output is accounted for by the prescribed dynamics. However, if the dynamics or forcing of such a model is inaccurate, its output may not be realistic. Conversely, a model that is guided to match observations will always produce realistic results but not necessarily for the right physical reasons. The HYCOM product used in this study belongs to the latter category. For this reason, the salinity variations produced by HYCOM will not perfectly obey the conservation equations within its own dynamical framework.

HYCOM guides its output to match observations through real-time data assimilation and relaxation to SSS climatology. The data assimilation scheme was summarized earlier and is described in full detail in Cummings (2005). For regions of the bay where the density of in situ salinity measurements is low, such as the Andaman Sea, data assimilation will have very little effect on the model's output. On the other hand, SSS relaxation occurs everywhere in the model's domain on relatively short time scales. SSS relaxation is implemented as

$$\frac{\partial S}{\partial t} = \frac{H_{\text{ref}}}{H} \left(\frac{S_c - S}{T_e} \right), \quad (10)$$

where S is the unadjusted model SSS, H is the MLD, H_{ref} is a reference MLD, T_e is the e -folding relaxation time scale, and S_c is the climatological SSS value. For these runs, H_{ref} and T_e were set to 30 m and 30 days, respectively (A. Wallcraft, U.S. Naval Research Laboratory, 2015, personal communication). With this formulation, the effective relaxation time scale increases with MLD. For a

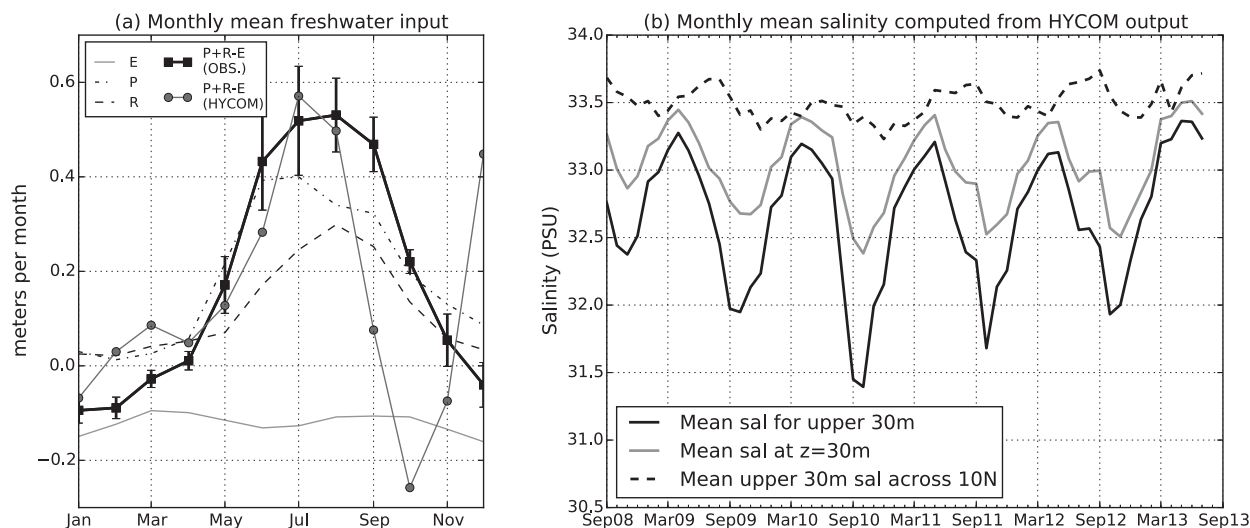


FIG. 7. (a) Monthly mean freshwater fluxes into the BoB, computed for the duration of the HYCOM runs used in this study (September 2008–July 2010). The gray line with circles represents the freshwater forcing used by HYCOM. The other lines show the freshwater flux computed from observations. The error bars on the $P + R - E$ (OBS.) line represent the standard error. The standard error is defined as σ/\sqrt{N} , where σ is the spatial standard deviation for a given month, and N is the effective spatial degrees of freedom determined by the principal component analysis method described in Bretherton et al. (1999). (b) Monthly mean salinities for the BoB region computed from HYCOM output: mean salinity for the upper 30-m BoB (black line), mean salinity at 30 m (gray line), and mean upper 30-m salinity across 10°N (broken line).

typical MLD of 20 m and an assumed average salinity difference ($S_c - S$) of 1 psu, the salinity tendency due to relaxation would be approximately $1.5 \text{ psu month}^{-1}$ in the model's surface layer. This means that the model's output is somewhat insensitive to its own freshwater forcing on seasonal time scales. This can be beneficial in instances where the model's freshwater forcing is uncertain or biased. We find this to be the case between September and December, a period when the model's freshwater forcing significantly diverges from observations (Fig. 7a). The cause of this inconsistency is unclear, but it points to inadequacies in the NOGAPS atmospheric forcing.

Since the model's SSS field strongly relaxes to observations on monthly time scales, we use observed monthly mean freshwater fluxes to construct our salinity budget. With this approach, we effectively take SSS adjustments due to relaxation as corrections to the model's freshwater forcing. This is justified in hindsight, as the observed freshwater forcing does a much better job of explaining the seasonal near-surface salinity variability produced by the model than the model's internal freshwater forcing.

Still, we acknowledge that data assimilation and SSS relaxation impose serious limitations on our study. In particular, strong relaxation to SSS climatology will suppress nonseasonal signals, such as those caused by ENSO and tropical cyclones. This process will also obscure small-scale structures in the horizontal eddy field that are not captured by climatology. For these reasons, we will

not use this HYCOM product to study interannual, sub-seasonal, or small-scale variability within the bay. That said, since HYCOM is effectively tuned to reproduce the observed, large-scale, seasonal salinity field of the ocean, we believe that this ocean state estimate is sufficient to assess the seasonal, basin-integrated, near-surface salinity balance for the BoB.

6. Controls on upper Bay of Bengal salinity budget

In this section, we take a more detailed look at the physical processes that control each term in our salinity budget. The ΔS_{fwf} term is mostly driven by the basin-integrated, net freshwater input. Precipitation P and river discharge R both peak during summer months, with maximum mean inputs of roughly 0.4 and 0.3 m month^{-1} , respectively (Fig. 7a). Total freshwater loss from evaporation is relatively flat throughout the year with a mean rate of about 0.1 m month^{-1} . We find that the integrated net freshwater input into BoB is about $4400 \text{ km}^3 \text{ yr}^{-1}$ or $0.14 \text{ Sverdrups (Sv)}$; $1 \text{ Sv} \equiv 10^6 \text{ m}^3 \text{ s}^{-1}$, which is in good agreement with the 0.13 Sv reported by Sengupta et al. (2006).

The ΔS_{mf} term will depend on the mean salinities along 10°N and the base of the control volume. According to HYCOM, mean salinity at 30-m depth is almost always less than the mean, upper 30-m salinity across 10°N (Fig. 7b). The greatest disparity occurs between October and November, when the salinity

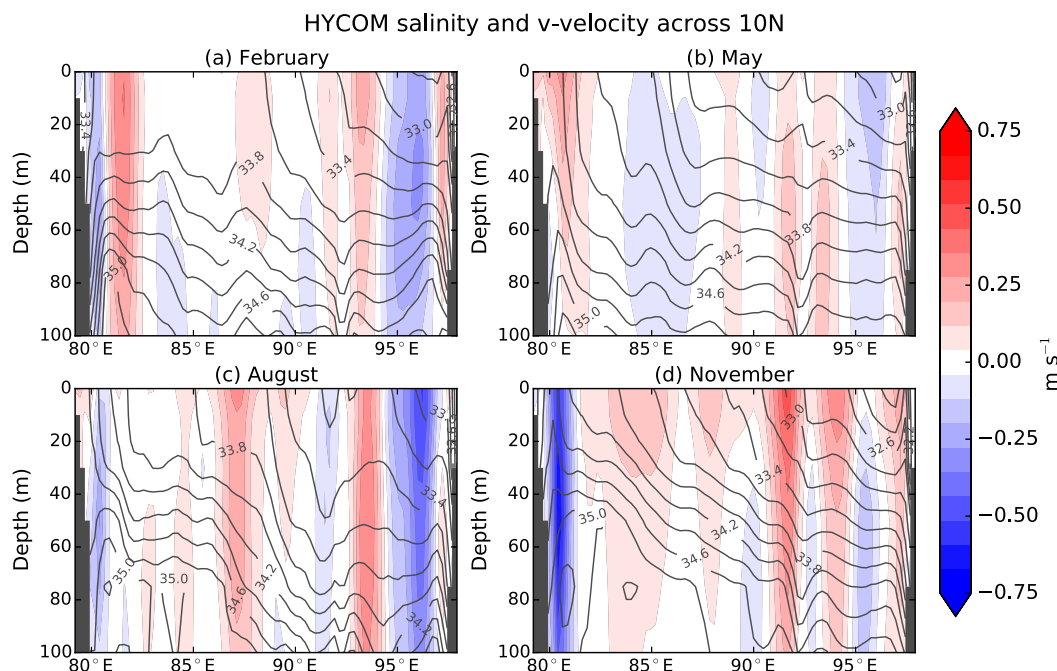


FIG. 8. Monthly mean northward velocity sections across 10°N from HYCOM output for (a) February, (b) August, (c) May, and (d) November. Solid contours represent monthly mean isohalines.

difference is as large as 1 psu; the credibility of this finding will be revisited later in the paper. In addition to the difference between the mean salinities across 10°N and $z = 30\text{ m}$, ΔS_{mf} will also depend on the horizontal mean flow across 10°N. Northward velocity estimates from HYCOM output show that the annual horizontal mean flow into the upper BoB is positive for most of the year, with the largest inflows occurring between October and December (Fig. 6). This mean northward flow into the upper layers of the bay is compensated by an equatorward flow at deeper levels (not shown). This also implies basinwide downwelling in the upper layers of the bay for most months of the year.

The ΔS_{hmix} term will depend on how salinity and northward velocity covary across 10°N. Across this line of latitude, salinity in the upper BoB generally decreases from west to east (Fig. 8). The associated pattern of northward velocity is characterized by bands of alternating currents (Fig. 8). The strongest currents are generally located near the coastlines of the bay, and they vary in amplitude and direction throughout the year. The EICC, centered at about 81°E, is most prominent in November when it flows equatorward with a maximum, near-surface velocity of about -0.75 m s^{-1} . In the Andaman Sea, the model produces a prominent equatorward flow along the eastern boundary for most of the year. This eastern boundary flow is strongest during summer months,

with peak velocities of about -0.5 m s^{-1} . However, we are unable to validate this finding with observations.

From Figs. 7, 6, and 8, we can predict the signs of ΔS_{hmix} and ΔS_{mf} . In November, for example, the strong equatorward EICC coupled with the negative eastward salinity gradient indicates that ΔS_{hmix} will be negative during that month. Additionally, since salinity across 10°N is always greater than the mean salinity at 30 m and the mean v velocity is usually northward, the ΔS_{mf} term will tend to be positive for most of the year.

7. Results from salinity budget analysis

a. Unadjusted salinity budget

Results from our salinity budget analysis show that the salinity change due to surface freshwater fluxes is the single largest driver of upper 30-m salinity variability in the bay (Fig. 9). As expected, ΔS_{fwf} mirrors the seasonality of the total freshwater input into the bay and has its largest effect between June and August. During those months, ΔS_{fwf} forces a mean salinity change of about $-0.5\text{ psu month}^{-1}$ in the upper 30 m. During the winter, when evaporation exceeds total freshwater input, ΔS_{fwf} has a maximum value of about $+0.15\text{ psu month}^{-1}$.

The salinity tendency due to horizontal mixing across 10°N, ΔS_{hmix} , is positive for most months of the year but is surprisingly negative in the late fall. This is the case

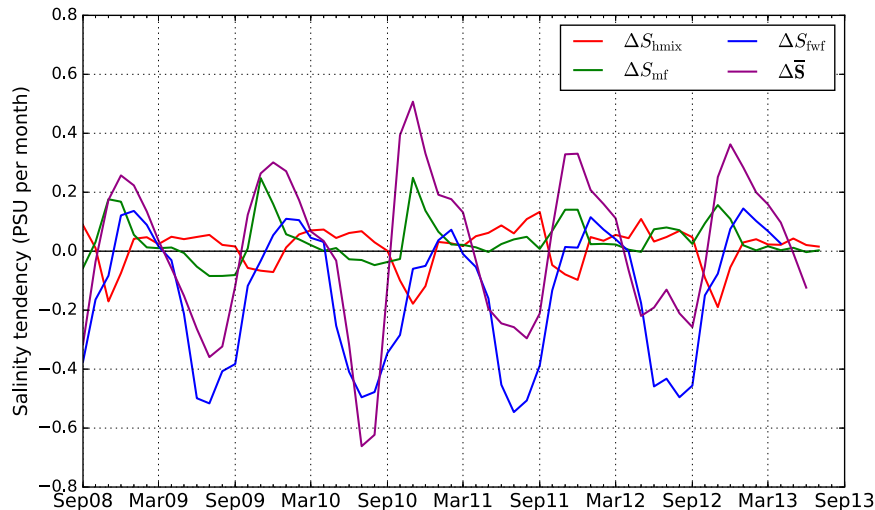


FIG. 9. Monthly mean time series of salinity tendencies for the upper 30 m of the BoB. The ΔS_{hmix} represents the upper BoB salinity tendency due to horizontal mixing across 10°N , ΔS_{mf} is the salinity tendency due to mean downwelling/upwelling in the upper bay, ΔS_{fw} is the salinity tendency due to surface freshwater fluxes, and $\Delta \bar{S}$ is the actual upper BoB salinity tendency diagnosed from the model. Each term is defined in Eq. (8). The term ΔS_{fw} was derived using observed freshwater fluxes. All other tendencies were derived from HYCOM output.

because HYCOM predicts that the water exported out of the bay by the EICC is more saline than the water flowing into the bay elsewhere (Fig. 8). Thus, in this scenario, the salinity flux of the EICC has the unexpected effect of making the upper bay fresher. The salinity tendency due to mean flow into the bay ΔS_{mf} is usually positive for most of the year, with peak values of $+0.1$ to $+0.25 \text{ psu month}^{-1}$ occurring between November and December. For some years, ΔS_{mf} is negative during the summer months. This occurs because there is a near-surface, equatorward mean flow out of the bay during those months for those years.

To get a better sense of how well the seasonal salinity budget balances, we sum the flux terms in Fig. 9 and compare their net to the total salinity tendency of the upper 30 m $\Delta \bar{S}$. Additionally, we make our comparisons more robust by regressing the monthly mean values from Fig. 9 onto a sinusoidal model containing the first three harmonics of the annual cycle. We define $\Delta S_{\text{FluxTotal}}$ as the sum of ΔS_{hmix} , ΔS_{mf} , and ΔS_{fw} . We also define $\Delta S_{\text{residual}}$ as $\Delta \bar{S} - \Delta S_{\text{FluxTotal}}$. For this seasonal salinity budget, $\Delta S_{\text{residual}}$ is relatively small between January and August (Fig. 10a). However, between September and December, $\Delta S_{\text{residual}}$ is relatively large and positive. During these months, the upper BoB experiences its most rapid increase in salinity but none of the computed flux terms can explain this increase.

If we assume that this residual is mostly due to salinity fluxes associated with vertical salt fluxes, we would conclude that ΔS_{vmix} is negligibly small for most of the year

except during the months that immediately follow the summer monsoon. This conclusion is physically reasonable as the vertical salinity gradient is relatively weak during the first half of the year but very strong during the months that follow the summer monsoon (Fig. 3). Even though a strong halocline would inhibit large overturns, weak mixing across a sharp gradient would still result in relatively large changes in near-surface salinities. This notion that the presence of a strong halocline could lead to enhanced rather than suppressed mixing was demonstrated by Akhil et al. (2014).

We can estimate the order of magnitude of the vertical eddy diffusion coefficient κ_z at 30 m by expressing ΔS_{vmix} as

$$\Delta S_{\text{vmix}} = -\frac{\kappa_z}{L_z} \frac{\partial \bar{S}^{x,y}}{\partial z}. \quad (11)$$

Between September and November, the average vertical salinity gradient at 30 m is $\sim 0.04 \text{ psu m}^{-1}$. Using $\Delta S_{\text{vmix}} \sim 0.3 \text{ psu month}^{-1}$ (estimated from the residual in Fig. 10a) and $L_z = 30 \text{ m}$, we get $\kappa_z \approx 1 \times 10^{-4} \text{ m}^2 \text{ s}^{-1}$. This of course is a rough estimate since κ_z is expected to vary spatially and temporally. Additionally, our estimate of κ_z is likely an upper limit of the true value, since Eq. (11) aggregates the effects of both turbulent mixing and advective vertical fluxes.

b. Adjusted salinity budget

The results presented thus far describe the upper bay salinity budget as simulated by HYCOM. While

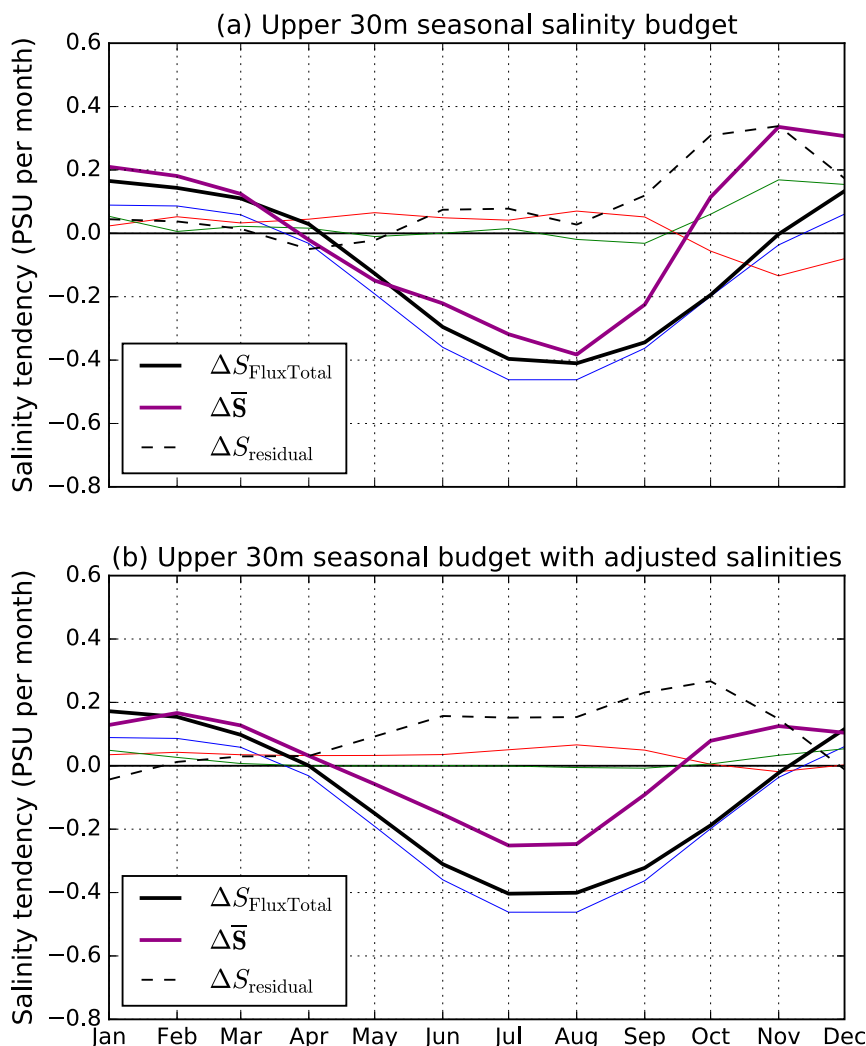


FIG. 10. (a) Seasonal salinity tendencies obtained by regressing the monthly tendency terms (Fig. 9) onto the first three harmonics of the annual cycle. (b) As in (a), but using the adjusted salinities described in the text. The red, blue, and green lines have their same meanings as in Fig. 9. The black line is $\Delta S_{\text{FluxTotal}}$, which is defined as the sum of ΔS_{hmix} , ΔS_{mf} , and ΔS_{fwf} . The term $\Delta S_{\text{residual}}$ is defined as $\Delta \bar{S} - \Delta S_{\text{FluxTotal}}$.

it is valuable to understand how the model behaves, our ultimate goal is to understand how the system works in nature. In an earlier section, we showed that there are significant differences between HYCOM's state estimates of salinity and the salinities' measurement by Argo profiling floats. Those findings cast uncertainty on some of HYCOM's predictions. We now try to assess how the results from the preceding analysis might change once we account for these biases.

To obtain robust estimates of the salinity biases shown in Fig. 5, we compute their monthly means within three overlapping subregions: BoB proper (BOBP), southern BoB (SBB), and southwestern BoB (SWBB). The BoB

proper subregion consists of all profile data north of 10°N (black dots in Fig. 4a). The SBB subregion includes all profile data between 8° and 12°N (orange crosses in Fig. 4a). The SWBB subregion accounts for the SBB profiles located roughly within 2° of latitude from the coastline between 10° and 12°N (blue x's in Fig. 4a). We choose these subregions because they have the most direct impact on our salinity budget. Plots of these regionally averaged biases are shown in Fig. 11. Interestingly, the upper 30 m of BoB proper has a negative salinity bias between September and December. This is surprising considering that HYCOM's internal freshwater forcing greatly underestimates the observed freshwater flux during this time (Fig. 7a). One possible

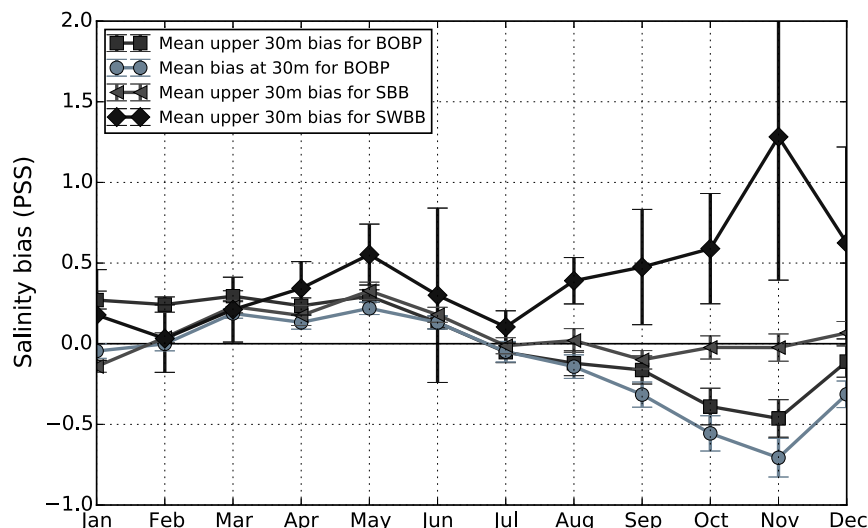


FIG. 11. Monthly mean HYCOM salinity biases for the BoB subregions defined in Fig. 4. The biases were computed from the monthly biases shown in Fig. 5. The error bars represent the 95% confidence interval of the plotted means based on a two-tailed Student's t test.

explanation for this discrepancy is sampling bias. There are relatively few profiles near coastal boundaries of the bay and almost none in the Andaman Sea. Therefore, it is possible that the Argo floats are undersampling the regions that have a positive salinity bias. Another possibility is that the SSS relaxation to climatology may have overcompensated for the low freshwater input during those months. In other words, if the true SSS values were higher than their climatological average, the model's relaxation scheme would introduce a fresh bias.

Next, we use the bias estimates for these subregions to make adjustments to the salinity terms in our budget. First, we use the upper 30-m salinity biases for BoB proper (black line in Fig. 11) to adjust the monthly means of \bar{S} . To do this, we subtract the monthly bias estimates from all corresponding monthly gridbox estimates that fall within the BoB proper region. For example, all salinity gridbox values that fall within the BoB proper region for the month of November would be adjusted by approximately 0.5 psu. We carry out similar procedures for all subregions and recompute the salinity terms in our budget. Since the profile data north of 20°N and in the Andaman Sea was so few, we do not adjust the salinities in those regions. These adjustments are obviously crude, but our goal is only to assess the sensitivity of our budget analysis to HYCOM's biases.

All salinity tendency terms except ΔS_{fwf} changed noticeably after applying the salinity adjustments (Fig. 10b). The changes to ΔS_{fwf} were negligible as the variability of this term is largely determined by the

variability of the freshwater fluxes, which we did not alter. As expected from Fig. 11, the most dramatic changes occurred between September and December. During those months, the amplitudes of the ΔS_{hmix} and ΔS_{mf} terms were greatly reduced. This occurred for two different reasons. First, after we corrected for the fresh bias at 30-m depth (gray line in Fig. 11), the difference between the salinities along 10°N and across the 30-m depth level all but vanished during those months. As a result, the amplitude of ΔS_{mf} was reduced to almost zero. Second, after we corrected for the positive salinity bias along the path of the EICC at 10°N, the equatorward salinity flux via the EICC roughly balances the northward salinity flux elsewhere. As a result, ΔS_{hmix} shifted toward zero. From this sensitivity analysis, we conclude that the peaks in ΔS_{hmix} and ΔS_{mf} observed between September and December (Fig. 10a) are largely artifacts of HYCOM's salinity biases.

The overall budget balance shifted in subtle ways after applying the salinity adjustments. After adjustment, $\Delta \bar{S}$ shifted to be less negative between May and August and less positive between September and December. Combined, these changes produce a more muted seasonal cycle for $\Delta \bar{S}$. The $\Delta S_{\text{residual}}$ is still negligibly small between January and April but now ranges between +0.1 and +0.25 psu month⁻¹ between May and November. If we again assume that $\Delta S_{\text{residual}}$ mostly captures the effect of vertical processes, we would conclude that vertical salinity fluxes have a major effect on near-surface salinities during and immediately following summer monsoon.

8. Summary

In this study, we establish a basin-integrated, seasonal salinity budget for the upper BoB using roughly 5 yr of data-assimilated HYCOM output. For our budget, we define an upper BoB control volume that accounts for the upper 30 m of the BoB region that is north of 10°N and inclusive of the Andaman Sea. Our near-surface salinity budget [Eq. (9)] consists of four salinity flux terms. These flux terms estimate the salinity tendency of the upper bay due to horizontal exchanges with the greater Indian Ocean ΔS_{hmix} , mean downwelling/upwelling in the upper Bay ΔS_{mf} , freshwater fluxes at the surface ΔS_{fwf} , and vertical exchanges across the base of the control volume ΔS_{vmix} . Since we have no reliable estimates of vertical mixing from the model, we inferred the importance of ΔS_{vmix} from the remaining terms in the budget.

We first assessed the basin-integrated, near-surface salinity budget without accounting for any biases in HYCOM's salinity field. From this analysis, we find that ΔS_{fwf} accounts for most of the near-surface salinity decrease during the summer monsoon and a significant portion of the salinity increase during the winter monsoon (Fig. 10a). However, ΔS_{fwf} could not explain the observed near-surface salinity increase between October and December. For this time period, our analysis yielded the surprising result that horizontal fluxes across 10°N act to decrease the mean near-surface salinity of the bay. This is because HYCOM (incorrectly) simulates a relatively saline EICC during this time. Overall, we find that our near-surface salinity budget, which excludes the effect of vertical mixing, approximately closes for all months except those immediately following the summer monsoon. For those excluded months, the sum of ΔS_{mf} , ΔS_{fwf} , and ΔS_{hmix} cannot explain the increase in mean near-surface salinity. From this result, we infer that vertical processes are likely driving the increase in near-surface salinity in the model for those months.

When we compare the model's gridbox salinity estimates with collocated in situ measurements from Argo profiling floats, we find coherent patterns of disagreements between the model's estimates and observations (Fig. 5). These differences or biases are largest during the months following the summer monsoon, particularly in November. Most notably, these comparisons show that HYCOM greatly overestimates the salinity of the EICC during the winter monsoon (Figs. 5, 11). With knowledge of these salinity biases, we made corrections to the salinity terms in our budget and reevaluated our results. After applying these adjustments, we find that the

observed upticks in the amplitudes of the ΔS_{hmix} and ΔS_{mf} terms between September and December (Fig. 10a) are mostly artifacts of HYCOM's salinity biases. As before, we find that the residual of our budget is still relatively large during postmonsoon months, implying a major role for vertical processes during those months.

9. Conclusions

From our basin-integrated, salinity budget analysis, we find that surface freshwater fluxes have the largest control on near-surface salinity over the BoB for most of the year. This finding is in agreement with other studies that have analyzed the variability of near-surface salinity for different subregions of the bay (e.g., Akhil et al. 2014; Pant et al. 2015). From this assessment, it follows that accurate knowledge of the bay's surface freshwater forcing is critical to any assessment of its near-surface salinity. Unfortunately, we find that HYCOM's internal freshwater forcing does not adequately reproduce the observed freshwater fluxes over the bay. As a result, the model relies heavily on SSS relaxation to keep its surface salinities consistent with observations. While these adjustments produced realistic seasonal variability, they compromised the model's ability to simulate non-seasonal signals and introduced biases where the SSS climatology is unreliable. We believe the latter contributed to the high-salinity bias along the path of the EICC during the winter monsoon. One immediate way to improve the model's performance in the BoB would be to replace its internal freshwater forcing with more reliable observationally based estimates. This could include the satellite-based river discharge estimates described in Papa et al. (2010).

Despite these shortcomings, HYCOM's ocean state estimates provide valuable insight into the processes that control upper BoB salinity. From our budget analysis, we deduce that vertical salt fluxes, across the base of the mixed layer, are largely responsible for counterbalancing the freshening of the near-surface layer caused by summertime freshwater fluxes. These results corroborate previous findings that highlight the importance of vertical mixing (e.g., Vinayachandran et al. 2013; Benshila et al. 2014; Akhil et al. 2014). The certainty of these results is undermined by the fact that HYCOM is likely overestimating the strength of vertical mixing in the upper 50 m of the bay. This is evidenced by the slight but persistent negative salinity biases observed below the mixed layer for most of the year (Fig. 5b). However, even after accounting for these biases, we still conclude that vertical salinity fluxes are necessary to close the near-surface salinity budget.

For our focus period, years 2008 to 2013, we find that horizontal salt fluxes across 10°N , in the upper 30 m, are not large enough to compensate for the huge freshening caused by surface freshwater fluxes. This holds true even after we accounted for the model's positive salinity bias along the path of the EICC. However, it is possible that the EICC could have a more prominent role under the right conditions. Recent studies have shown that the strength of the EICC and its ability to advect water from the northern regions of the bay are strongly affected by the phase of the Indian Ocean dipole (IOD; Pant et al. 2015; Chaitanya et al. 2015). During positive IOD events, the EICC is anomalously weak and low-salinity water remains trapped in the northern regions of the bay. Over our study period, there were three moderate positive IOD events (2008, 2011, and 2012) and one negative IOD event (2010) (Pant et al. 2015). Therefore, the EICC salt fluxes may have been anomalously weak during our study period.

Our results also cause us to speculate that the Andaman Sea is possibly a major outlet of low-salinity water from the BoB. Since the lowest-salinity waters are in the northeastern regions of the bay, the Andaman Sea provides a feasible avenue for low-salinity export. This is supported by our finding that HYCOM produces strong eastern boundary currents in the Andaman Sea that flow equatorward for most of the year (Fig. 8). However, we are unable to validate this conjecture since very little in situ data exist for this region.

The growing consensus among modeling studies that vertical mixing is important to the near-surface salinity balance needs to be bolstered by direct observational evidence. Currently, we have limited knowledge of the rates of vertical eddy diffusion within the bay. Output from high-resolution models, including HYCOM, shows that the upper bay is rife with sharp horizontal density gradients and submesoscale eddies. These small-scale features have the ability to support interesting mixed layer instabilities that modulate the mixing of all tracers (Boccaletti et al. 2007). Future modeling studies and observational work should examine these processes in more detail.

Acknowledgments. We thank the Program in Climate Change (PCC) at UW for providing support through the PCC Graduate Fellowship. We also thank NASA for support through Grants NNX09AU71G and NNX11AX79G, and NOAA/JISAO through Grants NA17RJ1232 and NA15OAR4320063. Additionally, we acknowledge that a portion of this work was funded through Office of Naval Research Grant N00014-15-1-2254. Finally, we express our gratitude to our two anonymous reviewers for their insightful and constructive feedback.

REFERENCES

- Akhil, V. P., and Coauthors, 2014: A modeling study of the processes of surface salinity seasonal cycle in the Bay of Bengal. *J. Geophys. Res. Oceans*, **119**, 3926–3947, doi:[10.1002/2013JC009632](https://doi.org/10.1002/2013JC009632).
- Barron, C. N., and L. F. Smedstad, 2002: Global river inflow within the Navy Coastal Ocean Model. *Proc. Oceans '02 MTS/IEEE*, Biloxi, MS, IEEE, 1472–1479, doi:[10.1109/OCEANS.2002.1191855](https://doi.org/10.1109/OCEANS.2002.1191855).
- Benshila, R., F. Durand, S. Masson, R. Bourdallé-Badie, C. de Boyer Montégut, F. Papa, and G. Madec, 2014: The upper Bay of Bengal salinity structure in a high resolution model. *Ocean Modell.*, **74**, 36–52, doi:[10.1016/j.ocemod.2013.12.001](https://doi.org/10.1016/j.ocemod.2013.12.001).
- Bleck, R., 2002: An oceanic circulation model framed in hybrid isopycnic-Cartesian coordinates. *Ocean Modell.*, **4**, 55–88, doi:[10.1016/S1463-5003\(01\)00012-9](https://doi.org/10.1016/S1463-5003(01)00012-9).
- Boccaletti, G., R. Ferrari, and B. Fox-Kemper, 2007: Mixed layer instabilities and restratification. *J. Phys. Oceanogr.*, **37**, 2228–2250, doi:[10.1175/JPO3101.1](https://doi.org/10.1175/JPO3101.1).
- Boyer, T. P., and Coauthors, 2013: *World Ocean Database 2013*. NOAA Atlas NESDIS 72, 209 pp.
- Bretherton, C. S., M. Widmann, V. P. Dymnikov, J. M. Wallace, and I. Bladé, 1999: The effective number of spatial degrees of freedom of a time-varying field. *J. Climate*, **12**, 1990–2009, doi:[10.1175/1520-0442\(1999\)012<1990:TENOSD>2.0.CO;2](https://doi.org/10.1175/1520-0442(1999)012<1990:TENOSD>2.0.CO;2).
- Chaitanya, A. V. S., and Coauthors, 2014: Salinity measurements collected by fishermen reveal a “river in the sea” flowing along the eastern coast of India. *Bull. Amer. Meteor. Soc.*, **95**, 1897–1908, doi:[10.1175/BAMS-D-12-00243.1](https://doi.org/10.1175/BAMS-D-12-00243.1).
- , and Coauthors, 2015: Observed year-to-year sea surface salinity variability in the Bay of Bengal during the 2009–2014 period. *Ocean Dyn.*, **65**, 173–186, doi:[10.1007/s10236-014-0802-x](https://doi.org/10.1007/s10236-014-0802-x).
- Chassignet, E. P., H. E. Hurlburt, O. M. Smedstad, G. R. Halliwell, P. J. Hogan, A. J. Wallcraft, R. Baraille, and R. Bleck, 2007: The HYCOM (Hybrid Coordinate Ocean Model) data assimilative system. *J. Mar. Syst.*, **65**, 60–83, doi:[10.1016/j.jmarsys.2005.09.016](https://doi.org/10.1016/j.jmarsys.2005.09.016).
- Cummings, J. A., 2005: Operational multivariate ocean data assimilation. *Quart. J. Roy. Meteor. Soc.*, **131**, 3583–3604, doi:[10.1256/qj.05.105](https://doi.org/10.1256/qj.05.105).
- D'Addezio, J. M., B. Subrahmanyam, E. S. Nyadjro, and V. S. N. Murty, 2015: Seasonal variability of salinity and salt transport in the northern Indian Ocean. *J. Phys. Oceanogr.*, **45**, 1947–1966, doi:[10.1175/JPO-D-14-0210.1](https://doi.org/10.1175/JPO-D-14-0210.1).
- Dai, A., and K. E. Trenberth, 2002: Estimates of freshwater discharge from continents: Latitudinal and seasonal variations. *J. Hydrometeor.*, **3**, 660–687, doi:[10.1175/1525-7541\(2002\)003<0660:EOFDFO>2.0.CO;2](https://doi.org/10.1175/1525-7541(2002)003<0660:EOFDFO>2.0.CO;2).
- Durand, F., D. Shankar, F. Birol, and S. S. C. Shenoi, 2009: Spatiotemporal structure of the East India Coastal Current from satellite altimetry. *J. Geophys. Res.*, **114**, C02013, doi:[10.1029/2008JC004807](https://doi.org/10.1029/2008JC004807).
- Girishkumar, M. S., M. Ravichandran, M. J. McPhaden, and R. R. Rao, 2013: Temperature inversions and their influence on the mixed layer heat budget during the winters of 2006–2007 and 2007–2008 in the Bay of Bengal. *J. Geophys. Res. Oceans*, **118**, 2426–2437, doi:[10.1002/jgrc.20192](https://doi.org/10.1002/jgrc.20192).
- Huang, R. X., 1993: Real freshwater flux as a natural boundary condition for the salinity balance and thermohaline circulation forced by evaporation and precipitation. *J. Phys.*

- Oceanogr.*, **23**, 2428–2446, doi:[10.1175/1520-0485\(1993\)023<2428:RFFAAN>2.0.CO;2](https://doi.org/10.1175/1520-0485(1993)023<2428:RFFAAN>2.0.CO;2).
- Large, W. G., J. C. McWilliams, and S. C. Doney, 1994: Oceanic vertical mixing: A review and a model with a nonlocal boundary layer parameterization. *Rev. Geophys.*, **32**, 363–403, doi:[10.1029/94RG01872](https://doi.org/10.1029/94RG01872).
- McPhaden, M. J., and Coauthors, 2009: RAMA: The Research Moored Array for African–Asian–Australian Monsoon Analysis and Prediction. *Bull. Amer. Meteor. Soc.*, **90**, 459–480, doi:[10.1175/2008BAMS2608.1](https://doi.org/10.1175/2008BAMS2608.1).
- Metzger, E. J., and Coauthors, 2014: US navy operational global ocean and Arctic ice prediction systems. *Oceanography*, **27**, 32–43, doi:[10.5670/oceanog.2014.66](https://doi.org/10.5670/oceanog.2014.66).
- Neetu, S., M. Lengaigne, E. M. Vincent, J. Vialard, G. Madec, G. Samson, M. R. R. Kumar, and F. Durand, 2012: Influence of upper-ocean stratification on tropical cyclone-induced surface cooling in the Bay of Bengal. *J. Geophys. Res.*, **117**, C12020, doi:[10.1029/2012JC008433](https://doi.org/10.1029/2012JC008433).
- Nyadjro, E. S., B. Subrahmanyam, V. S. N. Murty, and J. F. Shriver, 2010: Salt transport in the near-surface layer in the monsoon-influenced Indian Ocean using HYCOM. *Geophys. Res. Lett.*, **37**, L15603, doi:[10.1029/2010GL044127](https://doi.org/10.1029/2010GL044127).
- Pant, V., M. S. Girishkumar, T. V. S. Udaya Bhaskar, M. Ravichandran, F. Papa, and V. P. Thangaprakash, 2015: Observed interannual variability of near-surface salinity in the Bay of Bengal. *J. Geophys. Res. Oceans*, **120**, 3315–3329, doi:[10.1002/2014JC010340](https://doi.org/10.1002/2014JC010340).
- Papa, F., F. Durand, W. B. Rossow, A. Rahman, and S. K. Bala, 2010: Satellite altimeter-derived monthly discharge of the Ganga-Brahmaputra River and its seasonal to interannual variations from 1993 to 2008. *J. Geophys. Res.*, **115**, C12013, doi:[10.1029/2009JC006075](https://doi.org/10.1029/2009JC006075).
- Rao, R. R., and R. Sivakumar, 2003: Seasonal variability of sea surface salinity and salt budget of the mixed layer of the north Indian Ocean. *J. Geophys. Res.*, **108**, 3009, doi:[10.1029/2001JC000907](https://doi.org/10.1029/2001JC000907).
- Riser, S., J. Nystuen, and A. Rogers, 2008: Monsoon effects in the Bay of Bengal inferred from profiling float-based measurements of wind speed and rainfall. *Limnol. Oceanogr.*, **53**, 2080–2093, doi:[10.4319/lo.2008.53.5_part_2.2080](https://doi.org/10.4319/lo.2008.53.5_part_2.2080).
- Rosmond, T. E., J. Teixeira, M. Peng, T. F. Hogan, and R. Pauley, 2002: Navy Operational Global Atmospheric Prediction System (NOGAPS): Forcing for ocean models. *Oceanography*, **15**, 99–108, doi:[10.5670/oceanog.2002.40](https://doi.org/10.5670/oceanog.2002.40).
- Roullet, G., and G. Madec, 2000: Salt conservation, free surface, and varying levels: A new formulation for ocean general circulation models. *J. Geophys. Res.*, **105**, 23 927–23 942, doi:[10.1029/2000JC900089](https://doi.org/10.1029/2000JC900089).
- Schiller, R. V., and V. H. Kourafalou, 2010: Model river plume dynamics with the hybrid coordinate ocean model. *Ocean Modell.*, **33**, 101–117, doi:[10.1016/j.ocemod.2009.12.005](https://doi.org/10.1016/j.ocemod.2009.12.005).
- Sengupta, D., B. N. Goswami, and R. Senan, 2001: Coherent intraseasonal oscillations of ocean and atmosphere during the Asian summer monsoon. *Geophys. Res. Lett.*, **28**, 4127–4130, doi:[10.1029/2001GL013587](https://doi.org/10.1029/2001GL013587).
- , G. N. Bharath Raj, and S. S. C. Shenoi, 2006: Surface freshwater from Bay of Bengal runoff and Indonesian Throughflow in the tropical Indian Ocean. *Geophys. Res. Lett.*, **33**, L22609, doi:[10.1029/2006GL027573](https://doi.org/10.1029/2006GL027573).
- , B. R. Goddalahundi, and D. S. Anitha, 2008: Cyclone-induced mixing does not cool SST in the post-monsoon north Bay of Bengal. *Atmos. Sci. Lett.*, **9**, 1–6, doi:[10.1002/asl.162](https://doi.org/10.1002/asl.162).
- Sharma, R., N. Agarwal, I. M. Momin, S. Basu, and V. K. Agarwal, 2010: Simulated sea surface salinity variability in the tropical Indian Ocean. *J. Climate*, **23**, 6542–6554, doi:[10.1175/2010JCLI3721.1](https://doi.org/10.1175/2010JCLI3721.1).
- Shetye, S. R., A. D. Gouveia, D. Shankar, S. S. C. Shenoi, P. N. Vinayachandran, S. Sundar, G. S. Michael, and G. Nampoothiri, 1996: Hydrography and circulation in the western Bay of Bengal during the northeast monsoon. *J. Geophys. Res.*, **101**, 14 011–14 025, doi:[10.1029/95JC03307](https://doi.org/10.1029/95JC03307).
- Steele, M., R. Morley, and W. Ermold, 2001: PHC: A global ocean hydrography with a high-quality Arctic Ocean. *J. Climate*, **14**, 2079–2087, doi:[10.1175/1520-0442\(2001\)014<2079:PAGOHW>2.0.CO;2](https://doi.org/10.1175/1520-0442(2001)014<2079:PAGOHW>2.0.CO;2).
- Thadathil, P., P. M. Muraliedharan, R. R. Rao, Y. K. Somayajulu, G. V. Reddy, and C. Revichandran, 2007: Observed seasonal variability of barrier layer in the Bay of Bengal. *J. Geophys. Res.*, **112**, C02009, doi:[10.1029/2006JC003651](https://doi.org/10.1029/2006JC003651).
- TRMM, 2013: Daily TRMM and others rainfall estimate (3B42 V7 derived), version 7. Goddard Space Flight Center Distributed Active Archive Center, accessed 31 October 2013. [Available online at http://disc.sci.gsfc.nasa.gov/datacollection/TRMM_3B42_daily_V7.html.]
- Vecchi, G. A., and D. E. Harrison, 2002: Monsoon breaks and sub-seasonal sea surface temperature variability in the Bay of Bengal. *J. Climate*, **15**, 1485–1493, doi:[10.1175/1520-0442\(2002\)015<1485:MBASSS>2.0.CO;2](https://doi.org/10.1175/1520-0442(2002)015<1485:MBASSS>2.0.CO;2).
- Vinayachandran, P. N., V. S. N. Murty, and V. Ramesh Babu, 2002: Observations of barrier layer formation in the Bay of Bengal during summer monsoon. *J. Geophys. Res.*, **107**, 8018, doi:[10.1029/2001JC000831](https://doi.org/10.1029/2001JC000831).
- , D. Shankar, S. Vernekar, K. K. Sandeep, P. Amol, C. P. Neema, and A. Chatterjee, 2013: A summer monsoon pump to keep the Bay of Bengal salty. *Geophys. Res. Lett.*, **40**, 1777–1782, doi:[10.1002/grl.50274](https://doi.org/10.1002/grl.50274).
- Yu, L., X. Jin, and R. A. Weller, 2008: Multidecade global flux datasets from the objectively analyzed air-sea fluxes (OAFlux) project: Latent and sensible heat fluxes, ocean evaporation, and related surface meteorological variables. Woods Hole Oceanographic Institution Tech. Rep. OA-2008-01, 64 pp. [Available online at http://oafux.whoi.edu/pdfs/OAFlux_TechReport_3rd_release.pdf.]